3-27-2019

Tin Assisted Fully Exposed Platinum Clusters Stabilized on Defect-Rich Graphene for Dehydrogenation Reaction

Jiayun Zhang
Chinese Academy of Sciences

Yuchen Deng
Peking University

Xiangbin Cai
Hong Kong University of Science and Technology

Yunlei Chen
Chinese Academy of Sciences

Mi Peng
Peking University

See next page for additional authors

Comments

Authors

Jiayun Zhang, Yuchen Deng, Xiangbin Cai, Yunlei Chen, Mi Peng, Zhimin Jia, Zheng Jiang, Pengju Ren, Siyu Yao, Jinglin Xie, Dequan Xiao, Xiao-Dong Wen, Ning Wang, Hongyang Liu, and Ding Ma

Tin Assisted Fully Exposed Platinum Clusters Stabilized on Defect-rich Graphene for Efficient Dehydrogenation Reaction

*Jiayun Zhang,[1,2 #] Yuchen Deng,[3#] Xiangbin Cai,[4 #] Yunlei Chen,[5, 6 #] Mi Peng,[3] Zhimin Jia,[1,2] Zheng Jiang,[7] Pengju Ren,[5, 6] Siyu Yao,[3] Jinglin Xie,[3] Dequan Xiao,[8] Xiaodong Wen,[5, 6] Ning Wang,[4 *] Hongyang Liu,[1, 2 *] and Ding Ma,[3*]*

[1] Shenyang National Laboratory for Materials Science, Institute of Metal Research, Chinese Academy of Sciences, Shenyang 110016, P. R. China.

[2] School of Materials Science and Engineering, University of Science and Technology of China, Hefei 230026, P. R. China.

[3] Beijing National Laboratory for Molecular Sciences, College of Chemistry and Molecular Engineering and College of Engineering, and BIC-ESAT, Peking University, Beijing 100871, P. R. China.

[4] Department of Physics and Center for Quantum Materials, Hong Kong University of Science and Technology, Clear Water Bay, Kowloon, Hong Kong SAR, P. R. China.

[5] State Key Laboratory of Coal Conversion, Institute Coal Chemistry, Chinese Academy of Sciences, Taiyuan 030001, P. R. China.

[6] University of Chinese Academy of Science, No. 19A Yuanquan Road, Beijing 100049, P. R. China.

[7] Shanghai Institute of Applied Physics, Chinese Academy of Sciences, Shanghai 201204, P. R. China.

[8] Center for Integrative Materials Discovery, Department of Chemistry and Chemical Engineering, University of New Haven, 300 Boston Post Road, West Haven, Connecticut 06516, United States.

[#] These authors contributed equally to this work.

Corresponding authors: *Hongyang Liu (liuhy@imr.ac.cn), *Ning Wang (phwang@ust.hk) and *Ding Ma (dma@pku.edu.cn)

Keywords: Single-site Sn, Pt clusters, Atomic dispersion, Dehydrogenation, Butane activation

Abstract:

Atomically dispersed Pt clusters and single-site Sn are fabricated together on the core-shell nanodiamond@graphene (ND@G) hybrid support (a-PtSn/ND@G). This unique atomically dispersed Pt clusters can dramatically inhibit the side reactions and present excellent catalytic performance in direct dehydrogenation of n-butane at 450 °C, with >98% selectivity toward olefin products, in comparison with that of Al_2O_3 supported Pt_3Sn alloy nanoparticles (Pt_3Sn/Al_2O_3), due to the efficient utilization of Pt atoms and facile desorption of olefin. The combined results of density functional theory (DFT) calculation, HAADF-STEM and X-ray absorption fine structure (XAFS) results provide substantial insights that Pt clusters can be atomically dispersed and stabilized on the ND@G support by the assistance of single-site Sn species as a diluent agent and by the formation of Pt-C bond between Pt clusters and defective graphene nanoshell.

Introduction

Light olefins as one of the widely used feedstock in chemical industry are important building blocks for synthesis of chemical products.[1-2] Direct dehydrogenation (DDH) of light alkane as a typically industrial production process of these olefins undergoes an endothermic process, which requires high temperature to obtain satisfactory conversion rate and olefin yields, and it generally leads to serious catalyst deactivation by sintering of active sites and coking at higher reaction temperature.[1, 3] To-date, alumina-supported PtSn catalyst ($PtSn/Al_2O_3$) for dehydrogenation of light olefin is of wide research interest. As for $PtSn/Al_2O_3$ catalyst, the addition of Sn is crucial to obtain a better catalytic property in higher olefin selectivity and the formation of alloy Pt_3Sn can deliver better catalyst activity, while fast deactivation is still a main problem because the sintering of Pt_3Sn nanoparticles (NPs) cannot be effectively inhibited during dehydrogenation or reversed during regeneration process. Therefore, the development of highly dispersed and stabilized Pt-based catalyst is still urgent. [4-7]

In general, the support of catalyst plays an important role in Pt-based catalyst.[6, 8-10] Among the various supports, nanocarbons such as graphene-like materials have drawn much attention for their feasible fabrication of single site atom catalyst [11-17] and exhibit distinct catalytic performance in various reactions.[18-21] Nanodiamond is a unique nanocarbon material. After a facile thermal treatment, its surface can be reconstructed into an ultrathin, curved and defective sp^2 graphene nanoshell

reinforced by a sp^3 diamond nanocore (ND@G), which is beneficial for stabilizing metal NPs, through a strong metal-support interaction (MSI) between metal NPs and graphene nanoshell. [22-23]

Herein, we report a new Pt-Sn catalyst that consists of single-site Sn and atomically dispersed Pt clusters together anchored on the ND@G hybrid support (a-PtSn/ND@G). The as-prepared a-PtSn/ND@G catalyst provides enhanced DDH performance of n-butane in comparison with that of Al_2O_3 supported Pt_3Sn alloy nanoparticles (Pt_3Sn/Al_2O_3) which is normally considered responsible for higher activity in DDH reaction.[24] Multi-technique characterizations and DFT calculations results show that single-site Sn species deliver a dilution effect and Pt clusters are atomically dispersed among them through the linkage of Pt-C bond between Pt and graphene nanoshell. The as-prepared a-PtSn/ND@G catalyst dramatically inhibits the side reaction and shows distinct catalytic performance in DDH of n-butane at low temperature, resulting from the efficient use of Pt atom and the lower energy barrier for desorption of butene over these unique Pt clusters.

Results and discussion

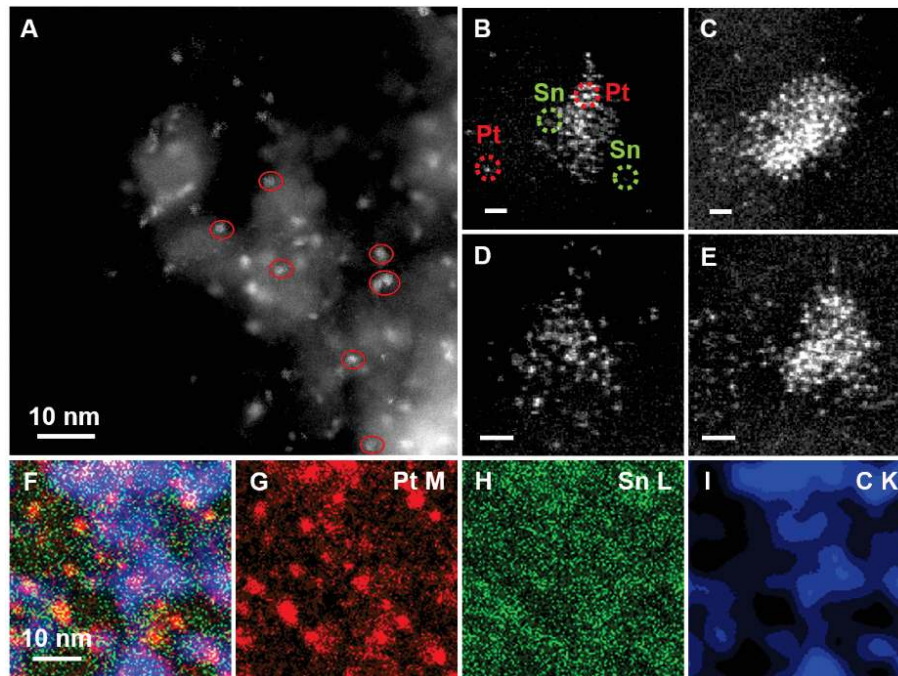Figure 1. HADDF-STEM characterization of a-PtSn/ND@G. **A**) STEM images showing the homogeneous distribution of Pt clusters and **B-E**) the atomic dispersion of Pt and Sn). For clarity, some Sn and Pt atoms in image **B** are marked out by green

and red circles according to the Z-contrast mechanism, respectively. (The scale bars in B-E are 0.5 nm). **F-I)** Energy-dispersive X-ray (EDX) spectroscopy showing the composition maps of the a-PtSn/ND@G.

The aberration-corrected high-angle annular dark-field scanning transmission electron microscopy (HAADF-STEM) was employed to study the dispersion of Pt and Sn on ND@G (**Figure 1**). Notably, Pt clusters were homogeneously decorated on ND@G as the light dots marked in **Figure 1 A** without any existence of Pt particles. The representative atomic images (**Figure 1 B-E)** showed that several Pt atoms formed a cluster as single atomic layer (**Figure S2**), while the single-site Sn atoms surrounded the Pt cluster in a random manner. The energy-dispersive X-ray (EDX) spectroscopy results (**Figure 1 F-I**) confirmed the coexistence and distinct distribution forms of Pt (red, clusters) and Sn (green, homogenous dispersion at atomic scale) on the support carbon (blue). A further H_2/O_2 titration measurement was performed (**Table S1**) and the result showed that for a-PtSn/ND@G, the dispersion of Pt is 99.2%, which is close to 100%, suggesting that almost all the Pt atoms are exposed on the surface of support. This result obviously supports the conclusion that ND@G can afford atomically dispersed Pt clusters. By contrast, Pt_3Sn alloy particles (d≈0.406nm, the lattice distance of Pt_3Sn (100) is 4.004 (PDF#65-0958)) on Al_2O_3 are observed rather than atomically dispersed Pt clusters (**Figure S3 A-E**). Composition analysis of Pt_3Sn/Al_2O_3 by EDX confirms the alloying of Sn and Pt (**Figure S3 F-I**). The dispersion of Pt on Pt_3Sn/Al_2O_3 is 74.7%, which is in good agreement with the calculation result from a theoretical model of 4 nm Pt_3Sn nanoparticle (**Table S1**).
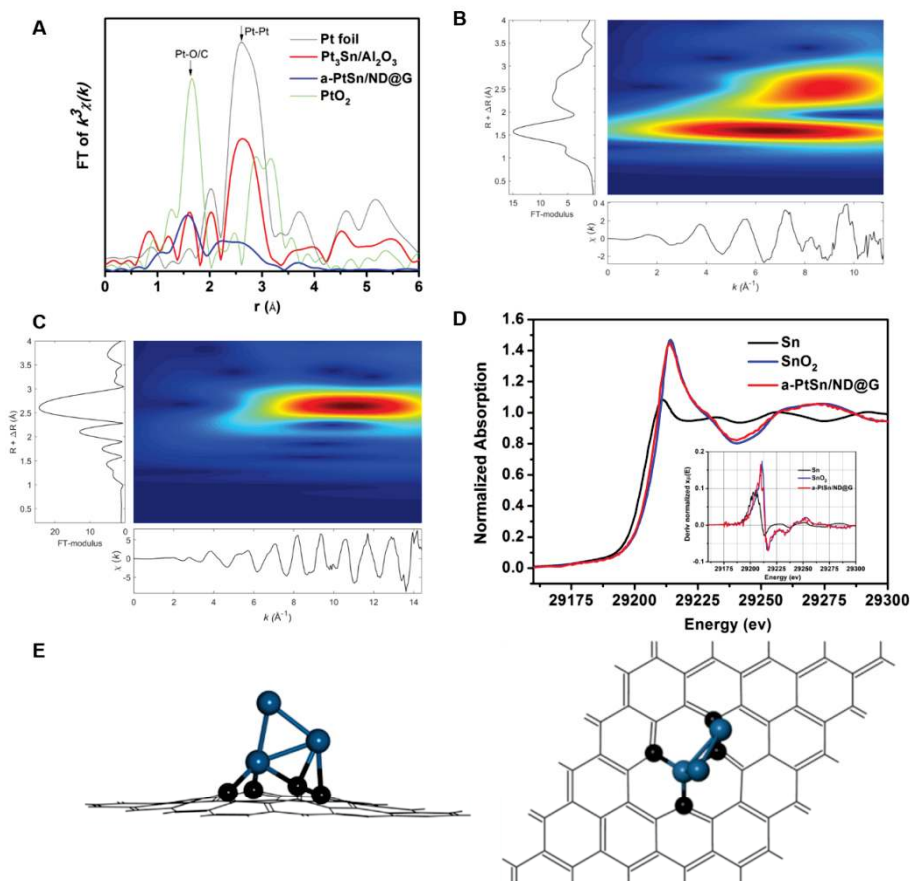
Figure 2. **A)** FT-EXAFS profiles for a-PtSn/ND@G, Pt_3Sn/Al_2O_3, Pt foil and PtO_2. **B)** Wavelet transform (WT) analysis of a-PtSn/ND@G and **C)** Pt_3Sn/Al_2O_3. **D)** XANES data characterizing Sn foil, a-PtSn/ND@G, and SnO_2. **E)** The optimized structure of Pt_3 cluster embedded into graphene (Pt_3-graphene) from top and side view, where the Pt-C bonds length is: 1.946, 1.977, 1.969, 2.046 and 2.301 Å.

The structure and the average coordination environment of Pt and Sn species were investigated by the extended X-ray absorption fine structure (EXAFS) spectroscopy. The Fourier-transformed (FT) k^3-weighted EXAFS at the Pt L_3-edge is shown in **Figure 2A**. For a-PtSn/ND@G catalyst, the distinct peak at 1.6 Å and the shoulder peak at 2.6 Å can be observed, corresponding to Pt-C and Pt-Pt first coordination shell, respectively. As for Pt_3Sn/Al_2O_3, the main peak at 2.6 Å belongs to Pt-Pt and Pt-Sn first coordination shell. Wavelet transformation (WT) of Pt L_3-edge EXAFS oscillations further illustrate the dispersion of Pt. Notably, the maximum WT intensity near 1.6 Å belongs to Pt-C contribution and another maximum at 2.6 Å corresponds to Pt-Pt contribution (**Figure 2B**), indicating the existence of Pt clusters anchored on the support by Pt-C in a-PtSn/ND@G catalyst. By contrast, only a

maximum at 2.6 Å can be observed for Pt_3Sn/Al_2O_3 (**Figure 2C**), revealing the formation of the Pt_3Sn alloy NPs on Al_2O_3 support. The detailed parameters of these two samples are shown in **Table S5**, **Figure S5 and Figure S6**. The collected results show that for a-PtSn/ND@G catalyst, the average coordination number (CN) of Pt-C contribution is 2.2, while the average CN of Pt-Pt contribution is only 1.8, which is much lower than that in Pt foil (CN of Pt-Pt is 12) and bulk PtO_2 (CN of Pt-O is 6) [25], confirming the presence of ultra-small Pt clusters on the ND@G. Meanwhile, the Pt-Sn contribution is absent, indicating that Pt species do not form Pt-Sn alloy. In addition, two Sn-O-Sn shell, with an average CN of 1.2 at a bond distance of 3.37 Å and 4.8 at a bond distance of 3.89 Å, are also presented and denoted as Sn-O-Sn_1 and Sn-O-Sn_2. The Sn-O coordination number is 5.9 at a bond distance of 2.05 Å and there is no Sn-Sn contribution. All these results further prove that the Sn species as single sites are also atomically dispersed on ND@G. Furthermore, the X-ray absorption near edge structure data indicates the existence of Sn as cationic species (**Figure 2D**). For Pt_3Sn/Al_2O_3, the presence of Pt-Sn coordination, the ratio of CN of Pt-Pt and Pt-Sn and the similar bond length of Pt-Pt and Pt-Sn suggest the existence of Pt-Sn alloy.

In order to further clarify the local coordination structure of Pt species, the density functional theory (DFT) calculation was used to investigate different bonding models of Pt-(C/O) on ND@G. As shown in **Figure 2E**, the optimized geometry of the Pt_3-graphene yields average bond length (2.05 Å) that is in good agreement with the experimental values of the Pt-C bond length (2.02±0.03 Å) in the first coordination shell. In addition, we exclude the possible PtO_x species embedded on the graphene in H_2 atmosphere. As shown in **Table S8-S10** and the reaction change of Gibbs free energies of Pt_3O_x-graphene in supporting information, oxygen can be captured easily by H_2 in the reaction condition. So, the most stable structure under reaction condition should be Pt_3 cluster stabled by graphene, which is applied in the further DFT calculations.

The electronic states of Pt species were investigated by X-ray photoelectron spectroscopy (XPS). As shown in **Figure S7A** and **Table S2**, Pt is completely in metallic state in Pt_3Sn/Al_2O_3 sample after reduction since the peak centered around 71.1eV (Pt $4f_{7/2}$) corresponds to Pt.[26-27] For a-PtSn/ND@G, the peak of Pt shows an upward shift trend in the binding energy (BE) compared to that of Pt_3Sn/Al_2O_3

(71.9eV vs 71.1 eV), which illustrates that Pt clusters trend to electron-deficient state in a-PtSn/ND@G. The XPS spectra of Sn is also presented in **Figure S7 B**, revealing that in a-PtSn/ND@G, Sn species in oxidation state Sn (II, IV), Thus, all the results above demonstrate that in a-PtSn/ND@G catalyst, several Pt atoms form a cluster of single atomic layer with electron-deficient, which is surrounded randomly by single-site Sn atoms as the dilute agent. And the Pt clusters are anchored on ND@G support through the linkage of Pt-C bond between Pt and graphene nanoshell.
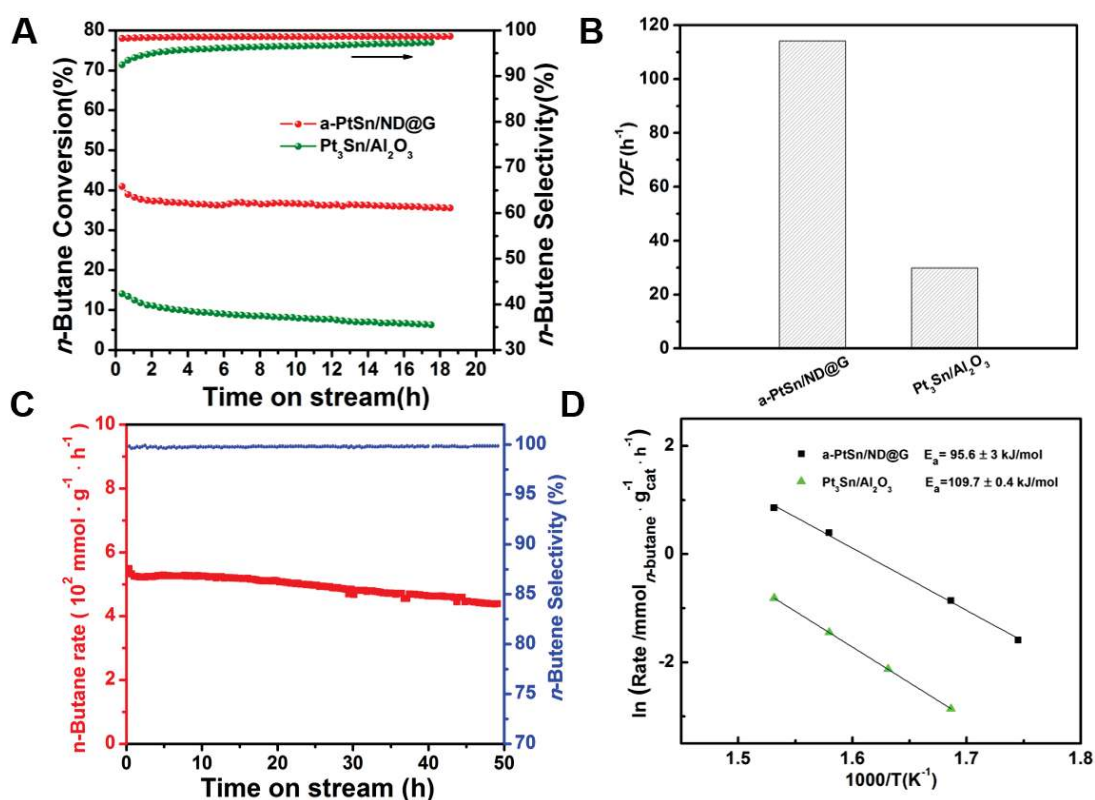

Figure 3. **A)** Conversion and selectivity by time-on-stream during DDH of n-butane at 450 °C. GHSV=18000 mL/g_{cat}·h, nC_4:H_2=1:1 with He as balancing gas. **B)** The turnover frequency (TOF) for a-PtSn/ND@G and Pt_3Sn/Al_2O_3. **C)** Stability test on a-PtSn/ND@G for n-butane dehydrogenation at 450 °C. GHSV=18000 mL/g_{cat}·h, nC_4:H_2=1:1 with He as balancing gas. **D)** Apparent activation energy (Eapp) of a-PtSn/ND@G and Pt_3Sn/Al_2O_3.

The catalytic performance of a-PtSn/ND@G and Pt_3Sn/Al_2O_3 for DDH of *n*-butane was evaluated under atmospheric pressure at 450 °C. As shown in **Figure 3A and Table S3**, the initial conversion of the Pt_3Sn/Al_2O_3 catalyst seriously decline from 14.1% to 6.3%, and the selectivity of total DDH products (TDP include n-butene, 1,

3-butadiene, ethylene and propylene) just reach 97.3% by the end of test. Deactivation on Pt_3Sn/Al_2O_3 is a typical behavior according to previous reported Pt based catalysts in the DDH of light alkanes which may result from coke deposition and/or sintering of active sites.[1] However, on a-PtSn/ND@G, the initial conversation of *n*-butane over is about 41% and the selectivity of TDP also reach 98.7%. In addition, the turnover frequency (TOF) of a-PtSn/ND@G ($114h^{-1}$) is approximately 3.7 times as that of Pt_3Sn/Al_2O_3 (**Figure 3B**). It should be noted that only a light deactivation after 18h test (from 41% to 35.7%) was observed. The atomic images of used a-PtSn/ND@G catalyst (**Figure S9**) show that the dispersion of Pt clustes and single-site Sn species on ND@G are still kept well after the long term test. The dispersion of Pt in the used a-PtSn/ND@G catalyst is 97.3% (**Table S1**), indicating that less Pt clusters are covered by coke and nearly all of them are still atomically exposed on ND@G. The long term stability of a-PtSn/ND@G (**Figure 3C**) shows a slight decrease in conversion rate (20%) after 50h test. Also, temperature programmed desorption of n-butene (n-C_4H_8-TPD, **Figure S10**) profiles demonstrate that the interaction between n-C_4H_8 and Pt clusters in a-PtSn/ND@G catalyst is weaker than that in Pt_3Sn/Al_2O_3 catalyst. This weak interaction means that a-PtSn/ND@G catalyst remains highly stable under the reaction conditions since coke formation covering metal sites is minimized during the DDH of n-butane. The apparent activation energy (Eapp) of a-PtSn/ND@G (**Figure 3D**) is also lower than that of Pt_3Sn/Al_2O_3 (95.6±3kJ/mol Vs 109.7±0.4kJ/mol), indicating different barriers of the reaction path which will be discussed in the following section. From the results above, it can be concluded that atomically dispersed Pt clusters on ND@G can deliver robust activity and stability in DDH of *n*-butane, which is superior to the previously reported Pt-based catalysts as displayed in **Table S4**.
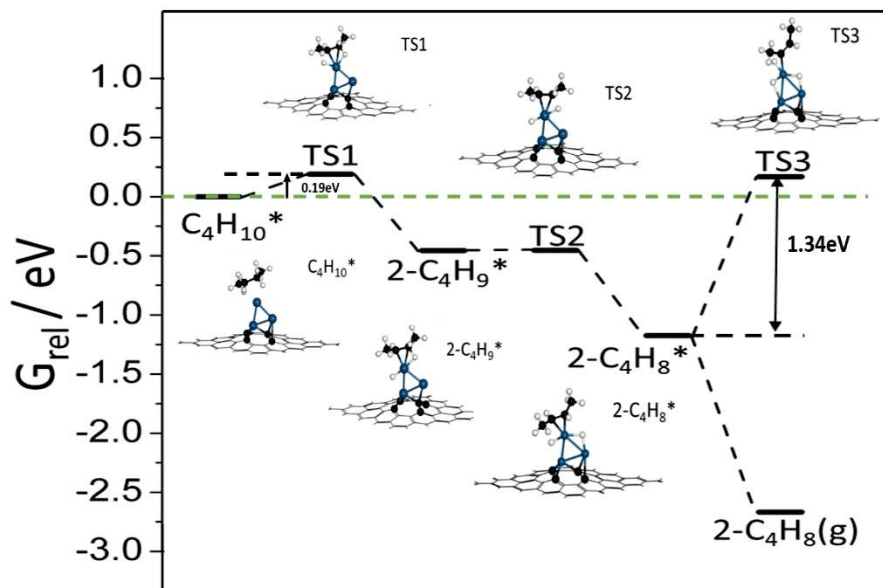
Figure 4. Gibbs free energy (T = 450 °C) profile of butane dehydrogenation on the Pt$_3$-graphene, and the structures for intermediates and transition states from C$_4$H$_{10}$ to 2-C$_4$H$_8$.

We also built the model of Pt clusters composed by three Pt atom on defective graphene named as Pt$_3$-graphene according to the deduced catalyst structures in EXAFS results (the average CN of Pt-Pt contribution is 1.8), and studied the reaction mechanism by quantum chemistry simulation at the DFT level. According to our experimental result, 2-butene is the main product in the DDH reaction, therefore we focus on the dehydrogenation barriers from n-butane to 2-butene in DFT calculation. In **Figure 4**, we consider the Gibbs free energy profiles at 723.15 K for the dehydrogenation of n-butane to 2-butene on Pt$_3$-graphene. As a comparison, the dehydrogenation mechanism of n-butane on Pt$_3$Sn-(111) is also considered (**Figure S11-S12**). The result of Pt$_3$-graphene is shown in **Figure 4**. In this catalytic system, butane dehydrogenation to produce 2-butene follows two steps. Firstly, the initial activation of n-butane occurs at methylene groups which generate 2-butyl (2-C$_4$H$_9$). Then 2-butene (2-C$_4$H$_8$) is formed via further dehydrogenation at methylene groups of 2-butyl.[28] As shown in **Table S6**, the key energy barriers for the forming of 2-butene and are 0.19 on Pt$_3$-graphene, 0.72eV on Pt$_3$Sn-(111), respectively, indicating the Pt$_3$-graphene is more active for the dehydrogenation of n-butane, which provides a rational interpretation of the high catalytic activity on a-PtSn-ND@G.

In addition, the deep dehydrogenation barrier of 2-butene on Pt$_3$-graphene and Pt$_3$Sn-(111) is 1.34, 0.69eV (**Figure 4, Figure S11 and Table S6**), and the desorption

barrier of 2-butene is of free energies at 723.15 K. The significant difference of deep dehydrogenation barrier indicates that the formation of deep-dehydrogenated intermediates, resulting in the coke deposition on active sites,[29-31] is more unfavorable on supported Pt_3 clusters. The calculation result indicates that the selectivity and stability performance of Pt_3-graphene will be better than Pt_3Sn alloy, which is in good agreements with our experimental observations. On atomically dispersed Pt_3 cluster on ND@G, the high selectivity results from the significant increasing of 2-butene deep dehydrogenation barriers and the high activity is guaranteed by low reaction barrier. The calculation is in good agreements with our experimental observations, where a-PtSn-ND@G shows better selectivity and stability performance than that of Pt_3Sn-Al_2O_3.

In conclusion, we demonstrated that atomically dispersed Pt clusters on ND@G exhibit enhanced catalytic performance for DDH of n-butane at a temperature as low as 450 °C. Multi-technique and DFT calculation results indicate that mono-dispersed Sn species work as a dilution agent and the linkage of Pt-C bond promotes the stabilization of Pt clusters on ND@G support. The lower energy barrier for the forming of 2-butene and the significant increased deep dehydrogenation barrier lead to the higher activity, better selectivity and stability of the a-PtSn/ND@G catalyst. This new catalyst design strategy offers a feasible way to prepare atomically dispersed Pt based catalyst and paves the way for rational design of highly active catalysts for direct dehydrogenation reaction.

References

1. Sattler, J. J. H. B.; Ruiz-Martinez, J.; Santillan-Jimenez, E.; Weckhuysen, B. M. *Chem Rev.* **2014**, *114*, 10613.

2. McFarland, E. *Science* **2012**, *338*, 340.

3. Xu, Y.; Lu, J.; Zhong, M.; Wang, J. *J. Nat. Gas Chem.* **2009**, *18*, 88.

4. Qiao, B.; Wang, A.; Yang, X.; Allard, L. F.; Jiang, Z.; Cui, Y.; Liu, J.; Li, J.; Zhang, T. *Nat. Chem.* **2011**, 3, 634.

5. Lin, L.; Zhou, W.; Gao, R.; Yao, S.; Zhang, X.; Xu, W.; Zheng, S.; Jiang, Z.; Yu, Q.; Li, Y. W.; Shi, C.; Wen, X. D.; Ma, D. *Nature* **2017**, *544*, 80.

6. Jones, J.; Xiong, H.; DeLaRiva, A. T.; Peterson, E. J.; Pham, H.; Challa, S. R.; Qi, G.; Oh, S.; Wiebenga, M. H.; Hernández, X. I. P.; Wang, Y.; Datye, A. K. *Science* **2016**, *353*, 150.

7. Nie, L.; Mei, D.; Xiong, H.; Peng, B.; Ren, Z.; Hernandez, X. I. P.; DeLariva, A.; Wang, M.; Engelhard, M. H.; Kovarik, L.; Datye, A. K.; Wang, Y. *Science* **2017**, *358*, 1419.

8. Shi, L.; Deng, G. M.; Li, W. C.; Miao, S.; Wang, Q. N.; Zhang, W. P.; Lu, A. H. *Angew. Chem. Int. Ed.* **2015**, *54*, 13994.

9. Zhu, Y.; An, Z.; Song, H.; Xiang, X.; Yan, W.; He, J. *ACS Catal.* **2017**, *7*, 6973.

10. Yao, S.; Zhang, X.; Liu; Zhou, W.; Gao R.; Xu, W.; Ye, Y.; Lin L.; Wen, X.; Liu, P.; Chen, B.; Crumlin, E.; Guo, J.; Zuo, Z.; Li, W.; Xie, J.; Lu, L.; Kiely, C. J.; Gu, L.; Shi, C.; Rodriguez, J. A.; Ma, D. *Science* **2017**, *357*, 389.

11. Lit, J. V. D.; Boneschanscher, M. P.; Vanmaekelbergh, D.; I jäs, M.; Uppstu, A.; Ervasti, M.; Harju, A.; Liljeroth, P.; Swart, I. *Nat Commun.* **2013**, *4*, 2023.

12. Ramasse, Q. M.; Seabourne, C. R.; Kepaptsoglou, D. M.; Zan, R.; Bangert, U.; Scott, A. J. *Nano Lett* **2013**, *13*, 498.

13. Wei, S.; Li, A.; Liu, J. C.; Li, Z.; Chen, W.; Gong, Y.; Zhang, Q.; Cheong, W. C.; Wang, Y.; Zheng, L.; Xiao, H.; Chen, C.; Wang, D.; Peng, Q.; Gu, L.; Han, X.; Li, J.; Li, Y. *Nat Nanotechnol.* **2018**, *13*, 856.

14. Chen, Z.; Vorobyeva, E.; Mitchell, S.; Fako, E.; Ortuño, M. A.; López, N.; Collins, S. M.; Midgley, P. A.; Richard, S.; Vilé, G.; Pérez-Ramírez, J. *Nat. Nanotechnol.* **2018**, *13*, 702.

15. Chen, Z.; Vorobyeva, E.; Mitchell, S.; Fako, E.; López, N.; Collins, S. M.; Leary, R. K.; Midgley, P. A.; Hauert, R.; Pérez-Ramírez, J. *Natl. Sci. Rev.* **2018**.

16. Yan, H.; Lin, Y.; Wu, H.; Zhang, W.; Sun, Z.; Cheng, H.; Liu, W.; Wang, C.; Li, J.; Huang, X.; Yao, T.; Yang, J.; Wei, S.; Lu, J. *Nat Commun* **2017,** *8*, 1070.

17. Mitchell, S.; Vorobyeva, E.; Perez-Ramirez, J. *Angew. Chem. Int. Ed.* **2018**.

18. Qiu, H. J.; Ito, Y.; Cong, W.; Tan, Y.; Liu, P.; Hirata, A.; Fujita, T.; Tang, Z.; Chen, M. *Angew. Chem. Int. Ed.* **2015**, *54*, 14031.

19. Yan, H.; Cheng, H.; Yi, H.; Lin, Y.; Yao, T.; Wang, C.; Li, J.; Wei, S.; Lu, J. *J Am Chem Soc.* **2015***, 137,* 10484.

20. Xie, S.; Tsunoyama, H.; Kurashige, W.; Negishi, Y.; Tsukuda, T. *ACS catal.* **2012**, *2*, 1519.

21. Vilé, G.; Albani, D.; Nachtegaal, M.; Chen, Z.; Dontsova, D.; Antonietti, M.; López, N.; Pérez-Ramírez, J. *Angew. Chem. Int. Ed.* **2015**, *54*, 11265.

22. Zhang, L.; Liu, H.; Huang, X.; Sun, X.; Jiang, Z.; Schlogl, R.; Su, D., *Angew. Chem. Int. Ed.* **2015**, *54*, 15823.

23. Liu, J.; Yue, Y.; Liu, H.; Da, Z.; Liu, C.; Ma, A.; Rong, J.; Su, D.; Bao, X.; Zheng, H., *ACS catal.* **2017**, *7*, 3349.

24. Deng, L.; Arakawa, T.; Ohkubo, T.; Miura, H.; Shishido, T.; Hosokawa, S.; Teramura, K.; Tanaka, T. *Ind. Eng. Chem. Res.* **2017**, *56*, 7160.

25. Zhu, Y.; An, Z.; He, J. *J. Catal.* **2016**, *341*, 44.

26. Serrano-Ruiz, J.C.; Sepúlveda-Escribano, A.; Rodríguez-Reinoso, F., *J. Catal.* **2007**, *246*, 158.

27. Morales, R.; Melo, L.; Llanos, A.; Zaera, F. J. *Mol. Catal. A-Chem.* 2**005**, *228*, 227.

28. Delbecq F, Sautet P. *Catal let.* **1994**, *28*: 89-98.

29. Forzatti, P.; Lietti, L. *Catal. Today* **1999**, *52*, 165.

30. Larsson, M.; Hultén, M.; Blekkan, E. A.; Andersson, B. *J. Catal.* **1996**, *164*, 44-53.

31. Bariås, O. A.; Holmen, A.; Blekkan, E. A. *Stud. Surf. Sci. Catal.* **1994**; *88*, 519.